JTTEE5 18:320–330
DOI: 10.1007/s11666-009-9329-y
1059-9630/$19.00 © ASM International

An Investigation on Powder Injection in the High-Pressure Cold Spray Process

T. Han, B.A. Gillispie, and Z.B. Zhao

(Submitted March 30, 2007; in revised form April 9, 2009)

High-pressure cold spray process is a relatively new coating process that uses high-velocity powder particles to form coatings. One of the requirements for this process is to inject the particles to be sprayed into a prenozzle chamber where both the particles and the powder feed gas are entrained into the primary gas stream. In this study, we investigated the effects of powder injection on coating formation through both experimental studies and computational simulations. Several issues related to powder injection will be examined, including the size of powder injector, the differential pressure, powder gas flow, and injector clogging. It is shown that an improved powder injector design not only enables the use of reduced amount of powder carrier gas flow but also maintains steady, clogging-free spraying conditions. Combining with properly selected injection conditions, it can also lead to enhanced coating deposition by kinetic spray process.

Keywords coating deposition, coating formation, high-pressure cold spray process, kinetic spray, powder injector, spray nozzle

1. Introduction

The high-pressure cold spray is a process that utilizes solid-state particles of various material types to form coatings (Ref 1-7). In this coating process, powder particles are accelerated by a supersonic gas stream generated by a de Laval-type spray nozzle. When the particles exit the nozzle at high velocities and impinge on a substrate, the powder particles undergo significant plastic deformations as a result of collisions and bond to the substrate and one another to form a coating. A schematic of the high-pressure cold spray nozzle is shown in Fig. 1(a). The powder particles to be sprayed are injected through a powder injector (made of a stainless steel tube), as shown in Fig. 1(b), into the prenozzle chamber where the powder particles and the powder carrier gas intermix with the primary gas. While the primary gas is typically heated to elevated temperatures, the gas flow carrying the particles from the powder feeder through the injector is at room temperature. Thus, the mixture of the primary gas and powder gas serves as the propellant gas that accelerates powder particles.

Coating formation by the high-pressure cold spray process is primarily controlled by particle velocities. Generally, there is a critical particle velocity for a given material being sprayed; particles above this velocity would stick to the substrate and particles below this velocity would bounce off or erode the substrate (Ref 2, 3). The key design variables include the temperature and pressure of the primary gas, the cross-sectional area of the nozzle throat, the nozzle standoff distance from a substrate, the surface condition of nozzle interior, and the powder gas flow. It was observed that the coating formation is largely controlled by two fundamental variables of the sprayed particles: particle velocity and particle temperature. The effects of different spray conditions on coating formation by the cold spray process can be generally interpreted through their influences on particle velocity and/or particle temperature. The ability to manipulate spray conditions of the kinetic spray process to maximize particle velocities is highly desirable to enhance the coating formation by the cold spray process. This is particularly true if one desires to use nitrogen or compressed air (instead of helium) as carrier gas and large size particles as feedstock. Particle temperature can also have strong effects on coating formation because most metallic materials being sprayed are softened at elevated temperature. Generally, a number of operating variables affect coating deposition by the high-pressure cold spray process to varying degrees through their influence on the velocity and temperature of sprayed particles (Ref 8, 9). Better understanding of the link between the process variables and coating formation is imperative to enhance the capability of the high-pressure cold spray as a coating process. While the temperature of the propellant gas is known as the primary variable that controls particle velocity and particle temperature, the effects of secondary variables have not been examined in detail. An earlier study suggests that decreased powder carrier gas flow, as a secondary variable in the high-pressure cold spray process, can be beneficial to the coating formations (Ref 8). However, there are limits on manipulating the flow of the powder gas due to the following reasons. First, the powder gas flow is primarily controlled by the size of powder injector and the

T. Han, GM R&D Center, Warren, MI 48090; **B.A. Gillispie**, Delphi Powertrain, Flint, MI 48556; and **Z.B. Zhao**, First Solar, Toledo, OH 43697. Contact e-mails: taeyoung.han@gm.com and bryan.a.gillispie@delphi.com.

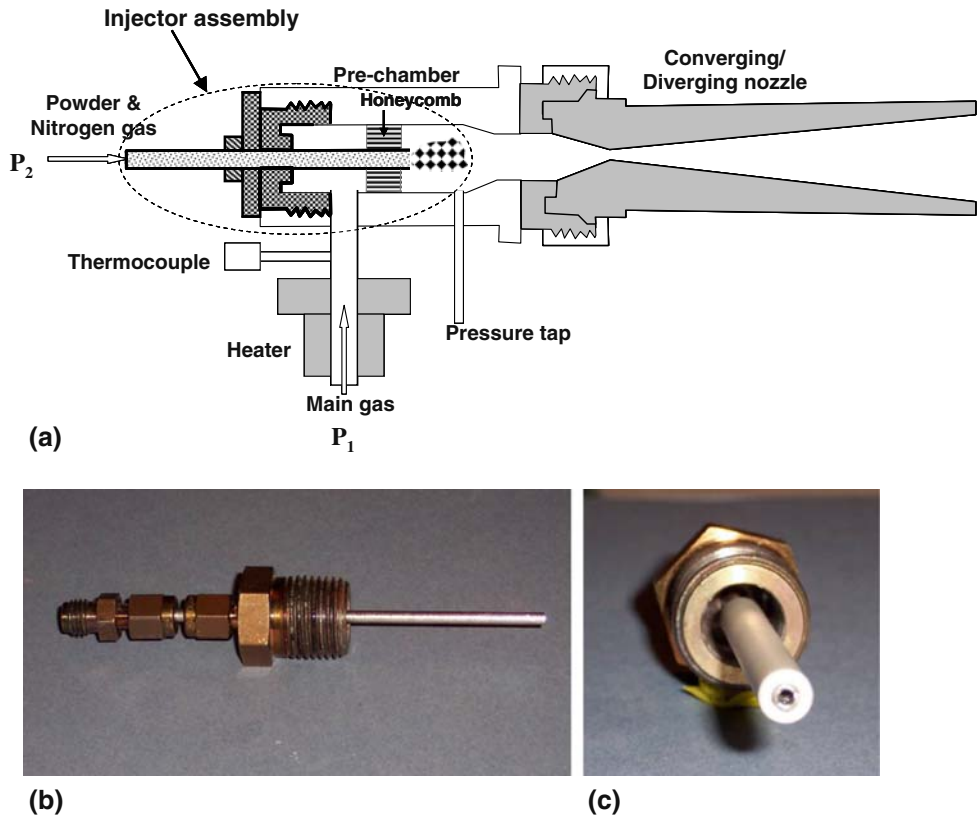

Fig. 1 Schematics of overall high-pressure cold spray: (a) Spray nozzle assembly, (b) A baseline powder injector assembly, and (c) Injector with Macor insulator

differential pressure ΔP ($\Delta P = P_2 - P_1$, see Fig. 1a). Injection of powder particles with a consistent powder flow rate stipulates a certain level of powder carrier gas flow. Second, powder clogging of injectors is directly linked to the powder gas flow, which can be explained by considering the high-pressure cold spray nozzle system shown in Fig. 1. It is noted that a significant segment of the powder injector tube is in direct contact with the primary gas (often at elevated temperatures up to 1000 K). Obviously, the injector, especially the segment that is immerged in the primary gas, is heated to elevated temperatures. The powder gas, which is at room temperature from powder feeder, can serve as a ''cooling'' agent for the injector and can counterbalance the heating from the outer surface that is exposed to the primary gas. Without sufficient powder gas flow, the powder injector becomes overheated and powder particles tend to stick to the inner wall of the injector tube. The accumulation of powder particles limits the powder gas flow and can eventually lead to complete injector clogging. This phenomenon can be particularly prevalent when compressed air or nitrogen (instead of helium) is used as the propellant gas for the high-pressure cold spray process, where the primary gas is heated to temperatures up to 1000 K to achieve sufficient particle velocities for coating formation.

In this study, we focused primarily on the aspects related to powder injection, the injector size, pressure differentials (i.e., $\Delta P = P_2 - P_1$ in Fig. 1a), and powder gas flow and their effects on coating formation. Both experimental studies and computational studies were conducted to investigate different powder injector configurations. The objectives of this study are twofold. One is to understand how powder injection affects the coating deposition process. The other is to optimize powder injector and injection parameters that enable one to use reduced powder gas flow while still maintaining steady powder injection and clogging-free spraying conditions. As it will be shown in this study, the optimization of the secondary variables (such as powder injection) can lead to enhanced sprayability by the high-pressure cold spray process. It is particularly beneficial for a coating process that uses compressed air or nitrogen (instead of helium) as the propellant gas when spraying hard materials and/or the powder materials with larger-sized particles.

2. Computational Method

2.1 Governing Equations

To better understand the basic mechanism of gas flow and heat transfer for the powder injector assembly, computational simulations were conducted in connection with experimental studies. Applying computational fluid

dynamics (CFD), the gas flow and heat transfer between the powder injector and the surrounding gas was simulated. The governing equations are the mass, momentum, and energy conservation equations for conjugate heat transfer between the gas phase and the solid phase of the injector. The governing equations for a compressible flow at a steady-state condition can be written in tensor notation as follows:

Conservation of mass

$$\frac{\partial(\rho u_i)}{\partial x_i} = 0 \qquad \text{(Eq 1)}$$

Conservation of momentum

$$\frac{\partial(\rho u_i u_j)}{\partial x_j} = -\frac{\partial p}{\partial x_i} + \frac{\partial \tau_{ij}}{\partial x_j} \qquad \text{(Eq 2)}$$

Conservation of energy for the gas phase

$$\frac{\partial(u_i(\rho E + p))}{\partial x_i} = \frac{\partial}{\partial x_j}\left(k_{\text{eff}}\frac{\partial T}{\partial x_i} + u_j \tau_{ij}\right) - S_{\text{h}} \qquad \text{(Eq 3)}$$

Conservation of energy for the solid phase

$$k_{\text{s}}\frac{\partial T_{\text{s}}^2}{\partial x_i^2} + S_{\text{h}} = 0 \qquad \text{(Eq 4)}$$

where x_i ($i = 1,2,3$) are independent space variables, ρ, u_i, p, τ, E, k_{eff}, and T are fluid density, velocity, pressure, shear stress, internal energy, effective conductivity, and temperature of the gas phase, respectively. For the solid phase, C_p, T_{s}, k_{s}, and ρ_{s} are specific heat, temperature, thermal conductivity, and density of the stainless steel injector, respectively. S_{h} is the heat transfer rate at the interface between the gas flow and the injector tube. The heat transfer occurs simultaneously at both inside and outside regions of the injector. Due to a high Reynolds number based on the tube diameter ($\text{Re}_{\text{d}} \cong 11.2 \times 10^5$), the gas flow in the computational domain was assumed as fully turbulent. To account for turbulence in the flow, a standard k-ε turbulence model (Ref 10) was employed with a standard wall function (Ref 10). As the gas flow is compressible, the density variations in the field were predicted based on the laws for an ideal gas.

For the majority of work in this study, we focused mainly on the heat transfer between the gas flow phase and the injector assembly neglecting the effects of powder particles. To explain the enhanced coating formation covered in section 4.4, we also simulated the gas flow with a discrete particle model to track the particles injected in the powder gas flow. Depending on powder feed rate, the main gas flow can influence discrete particles and vice versa. Therefore, the interaction of particles with the gas flow was taken into consideration in later simulations. In a coupled approach, calculations of the gas flow phase and the discrete particle phase were alternated until a converged coupled solution is achieved. The details of the physical models for discrete particle interactions with turbulent flows were described in our previous work (Ref 8).

2.2 Computational Domain and Boundary Conditions

In this study, our simulations were around the injector assembly, and the computational domain was limited to the prechamber of the high-pressure cold nozzle system. The flow and heat transfer around the injector is axisymmetric, and a computational model for an axially symmetric injector was generated to simulate gas flow and heat transfer around the powder injector as shown in Fig. 2. An air gap with thickness of ~100 μm between the stainless tube and the ceramic tube was included in the model for conduction heat transfer analysis without air flow simulations in the air gap. The CFD code FLUENT (Ref 11) is capable of handling heat transfer between the gas phase and the solid phase via conjugate heat transfer.

In the present simulations, the prechamber was specified as a stainless steel cylinder with an inside diameter of 15 mm, and an adiabatic heat transfer boundary condition was applied on the outer surface of the prechamber for simplicity. The stainless steel tubes for powder injector had the wall thickness of 0.73 mm. For boundary conditions of the primary gas flow, the pressure and temperature were specified according to the values that were measured at the prechamber inlet for the given spray conditions. For the powder gas flow for the injector, the measured mass flow rate and the temperature were specified at the inlet of the powder injector. Turbulence intensity of 10% was assumed at the inlets of the powder gas flow and the main gas flow. The turbulence length scale of 1 and 2 mm were assumed at the inlets of the powder gas flow and the main gas flow, respectively. These inlet turbulence quantities may influence the flow field near the inlet, but the standard k-ε turbulence model (Ref 10) corrects these turbulence quantities based on local turbulence production and the dissipation in the downstream of the inlet. The temperature of the powder gas was assumed to be 350 K. At the solid walls, the no-slip condition was used with the standard turbulent wall function (Ref 10) and the conjugate heat transfer was implied between the injector stainless tube and the surrounding gas flows. For the exit boundary conditions, a constant pressure boundary condition was specified and a zero temperature gradient boundary condition was specified where the flow is subsonic. The total number of finite volumes was about 7000 quad elements for an axisymmetric model. The accuracy of the present computational method for high-pressure cold spray applications has been discussed in Ref 8, 12, 13. More detailed validations for 3D turbulent flows are under investigation and will be reported in future publications.

2.3 Material Properties

As will be detailed in the following sections, several injector configurations were designed to vary the powder gas flow while minimizing the injector clogging. In addition to the bare stainless steel tube, powder injectors encapsulated with a hollow ceramic (Macor) sleeve (see Fig. 1c) were also examined. We decided to use

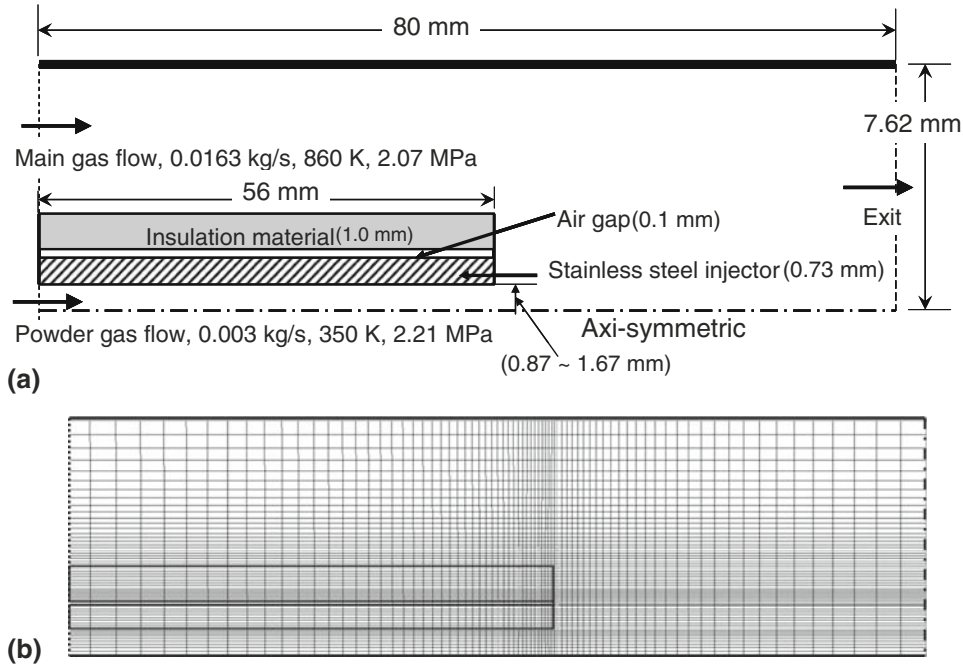

Fig. 2 A computational domain for the injector assembly analysis: (a) Schematics of computational domain with specific dimensions and (b) Computational mesh for axisymmetric model

Table 1 Material properties for gas and solids

Properties	Stainless steel (T 600 series)	Aremco Macor (machinable glass ceramic)	Nitrogen
Density, kg/m^3	8030	2520	Ideal gas law
Specific heat (C_p), J/kg · K	502.5	790	1040
Thermal conductivity, W/m · K	16.3	1.46	0.0242

Macor (Machinable Glass Ceramic manufactured by AREMCO) due to machinability with ordinary metal working tools and it holds tight tolerances and withstands high temperature environments up to 1300 K with relatively low thermal conductivities. The present computational model with conjugate heat transfer predicts the temperature distribution of the stainless steel tube, the Macor sleeve, and the powder carrier gas inside the injector. The material properties used in the simulation for the conjugate heat transfer and the gas flows are listed in Table 1.

3. Experimental Procedures

The high-pressure cold spray facility at Delphi Research Labs was used for the experimental studies of coating deposition. A detailed description of the high-pressure cold spray process and the facility was reported previously (Ref 5-9). The aluminum-silicon alloy powder

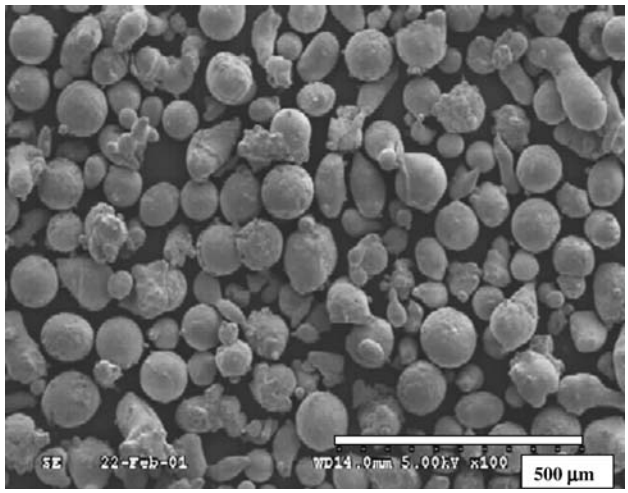

Fig. 3 Morphology and size distribution (53 to 105 µm) of the Al-Si alloy powder used in this study

was prepared using a gas atomization process. The particle size distribution of the powders was 53 to 103 µm, and their morphologies are shown in Fig. 3. The feedstock powders were injected into the spray nozzle using a high-pressure powder feeding system with a calibrated powder feed rate. The primary gas was compressed nitrogen at 2.07 MPa (300 psi). The nitrogen pressure at the powder feeder was kept at higher pressures from 2.21 MPa (320 psi) to 2.40 MPa (350 psi). This allowed a positive powder gas flow into the prenozzle chamber where both

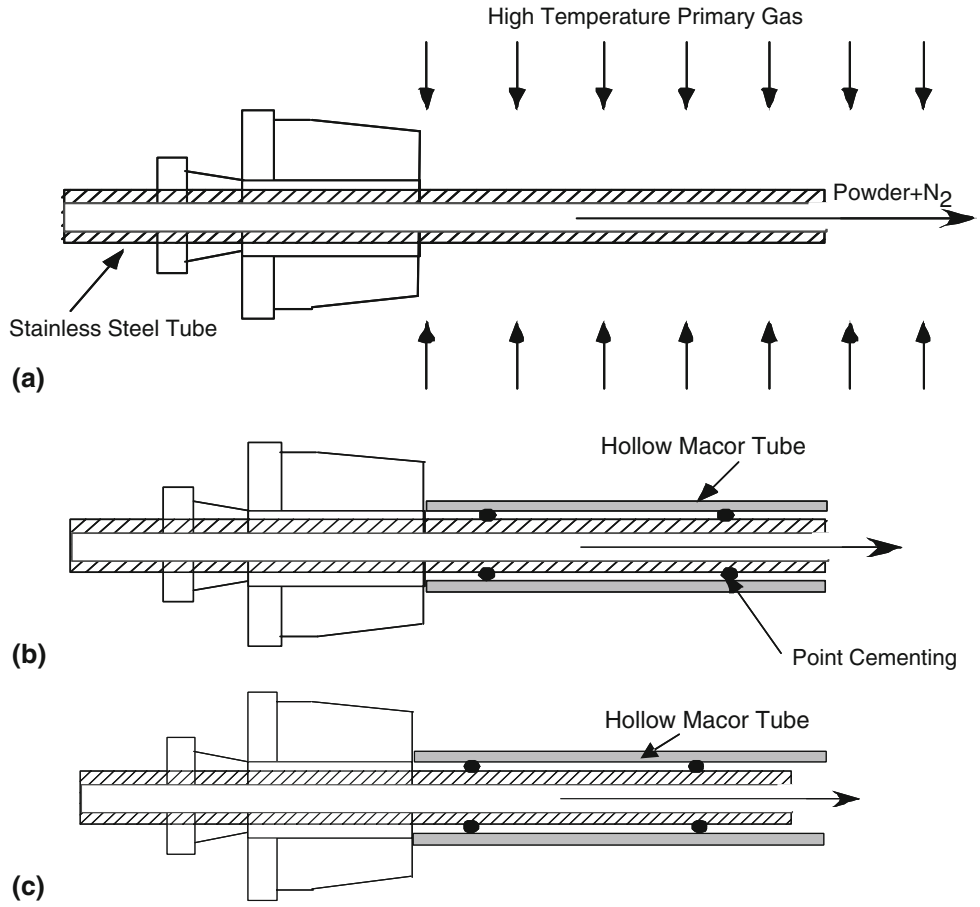

Fig. 4 Several injection configurations examined in this study: (a) An injector made of bare stainless steel tube without insulation, (b) An injector in which the stainless steel tube is encapsulated with a hollow Macor tube, and (c) A recessed injector configuration

Table 2 Powder injection parameters for three case studies with the injector configuration shown in Fig. 4(c)

Case studies	Tube diameter, mm	Pressure differential (ΔP), MPa	Powder gas flow, g/s	Primary gas pressure (P_1), MPa	Powder feed rate, g/s
1	3.34	0.28	16.5	2.07	1.1
2	1.74	0.28	8.9	2.07	1.1
3	1.74	0.14	4.7	2.07	1.1

the sprayed particles and the powder gas flow become intermixed with the primary gas stream. Aluminum alloy substrates were mounted on a computer-controlled XYZ stage, in this study. During coating deposition, the substrates were translated at controlled traverse speeds in front of the spray nozzle. The loading of a deposited coating was determined by measuring the weight of the sample before and after deposition.

During the experiments, several configurations of the injector assembly were examined. Stainless tubes with two different inside diameters were used for the injector assemblies: $D_1 = 1.74$ mm and $D_2 = 3.34$ mm. These injector configurations are shown in Fig. 4. Previously, an injector with a stainless steel tube without the insulation, as shown in Fig. 4(a), has been commonly used in the high-pressure cold spray process. The new injector assembly consists of stainless steel tube that was encapsulated with a hollow ceramic (Macor®) tube (thermal conductivity, 1.46 W/m · K) and an air gap with thickness of ~100 μm between the stainless tube and the ceramic tube. The typical test conditions are listed in Table 2 and the detailed descriptions of these injectors are given in the following sections.

4. Results and Discussion

4.1 Injector Clogging-Related Issues

For the injector configuration shown in Fig. 4(a), two different sizes of the injectors (inside diameters, $D_1 = 1.74$ mm and $D_2 = 3.34$ mm) were examined. Under

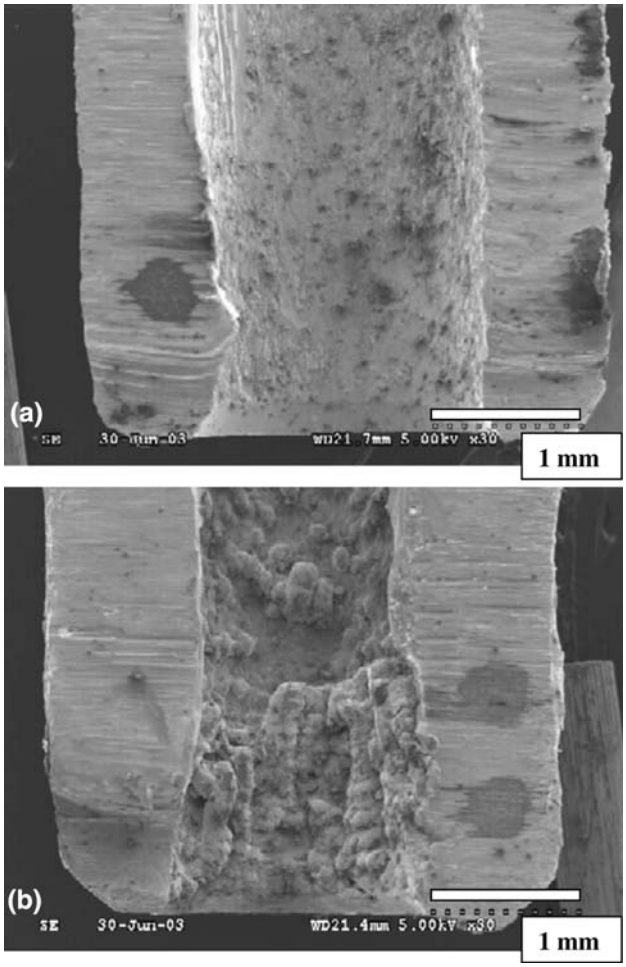

Fig. 5 SEM micrographs showing the interior surface of a powder injector: (a) The interior surface of the new injector (not used) and (b) The interior surface of a nearly clogged injector

similar spray conditions, the small injector, which is apparently associated with reduced powder gas flow, generally led to improved coating depositions, namely high mass loadings and deposition efficiencies. However, the small injectors are often prone to particle buildup on their interior wall surface which introduces injector clogging. This can be especially prevalent when using compressed air or nitrogen for coatings of difficult-to-spray materials (materials that are harder than pure Al or Cu, etc.). In this case, the primary gas is often heated to elevated temperatures (up to 1000 K) to increase both the particle temperature and the particle velocity, in order to have reasonably high deposition efficiencies. Apparently, this can cause overheating of the powder injector since it is in direct contact with the primary gas in the prenozzle chamber, as shown in Fig. 4(a). When powder particles are injected through a stainless steel injector into the hot primary gas stream, from the test results, some of them tend to adhere to the overheated inner surface of the stainless steel tube (see the example in Fig. 5b). As a result of the powder particles buildup inside the injector, the effective flow area is reduced, which causes continuous

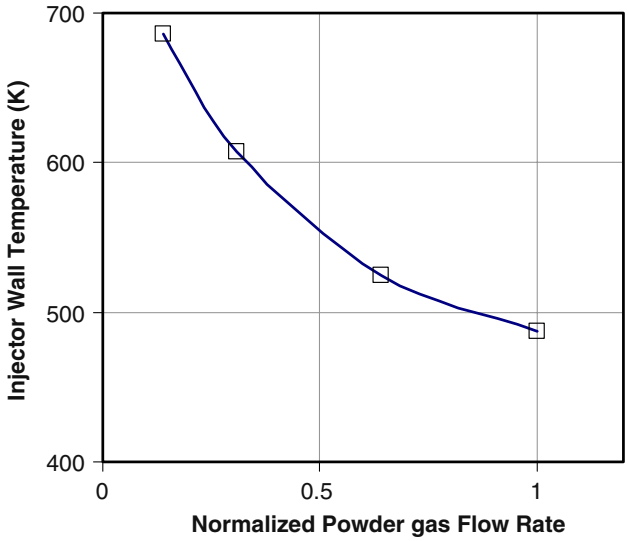

Fig. 6 A simulation result illustrating the effect of powder gas flow rate for the injector configuration shown in Fig. 4(a) with the smaller injector ($D_1 = 1.74$ mm) on the temperature at the inner wall of the powder injector (operating conditions are the same as shown in Fig. 2, except the powder gas flow rate is decreased from the base line of 0.003 to 0.0005 kg/s)

decrease in powder gas flow. The effect of the powder gas flow on the injector wall temperature was simulated for the injector configuration shown in Fig. 4(a) with the smaller injector (D_1 = 1.74 mm), and the result is illustrated in Fig. 6. The average injector wall temperature increases rapidly as the powder gas flow decreases. The result is mainly due to diminished cooling effect by the powder gas flow on the injector (note that the powder gas is kept at room temperature). When the injector temperature increases, the particle buildup is accelerated. This causes continuous deviations of powder gas spray parameters from the operating set-points and eventually can result in complete clogging of the injector. For example, when spraying the Al alloys at the primary gas temperature of 870 K with the small injector, one has to clean or replace the small injector after every 2 to 10 min of spray time depending on the other spray conditions. While this makes laboratory experiments very difficult due to constant interruptions, it is totally unacceptable in a potential production environment that utilizes the high-pressure cold spray process.

One way to minimize or prevent the injector from clogging is to lower the injector wall temperatures. In principle, this can be achieved by increasing the cooling by simply increasing the pressure differential ($\Delta P = P_2 - P_1$) to increase powder gas flow. Practically, however, this would lead to reduced coating formation by the high-pressure cold spray process. Since the powder gas is at room temperature and mixed with the primary gas, the increase in the powder gas flow would lower the effective temperature of the propellant gas, which degrades coating formation by lowering particle temperatures and particle velocities. Therefore, simply increasing the powder gas flow would not be a desirable solution. Several new

configurations of injectors, with Macor insulation, were examined to allow the use of minimum amounts of powder gas flows for better coating formation, while maintaining non-buildup conditions in the powder injector. Macor is easy for machining and withstands high-temperature environments up to 1300 K with relatively low thermal conductivities. Detailed descriptions of the new injector configurations and related powder gas flow and gas temperature distributions are described in the following sections.

4.2 Effects of Thermal Insulation of the Injector

As shown in Fig. 4, the stainless steel injector was encapsulated by a hollow ceramic (Macor) tube with a relatively low thermal conductivity (~1.46 W/m · K). In this study, the several thicknesses of Macor hollow tube were examined to understand the effects of thermal insulation. A small air gap between the stainless steel injector and the ceramic tube was intentionally introduced. The air gap is required to improve the thermal insulation and also to prevent fractures of the ceramic tube due to different thermal expansion rates between the stainless steel tube and the Macor tube. Without the air gap, a good thermal insulation was not achieved. This can be explained from the analytical solution for the critical radius of insulation (Ref 14).

Considering a tube of ceramic insulating material with inside radius r_i at a constant temperature T_i and the outside surface of the insulation with a radius r_o exposed to a gas flow at a temperature T_h, the total heat transfer rate in the radial direction per unit length of the tube (Ref 14) is,

$$q = \frac{2\pi(T_h - T_i)}{\frac{1}{h_o r_o} + \frac{1}{k}\ln\left(\frac{r_o}{r_i}\right)} \quad \text{(Eq 5)}$$

where h_o is the coefficient of heat convection at the outside surface of the insulation and k is the thermal conductivity of the insulating material. If we assume that T_h, T_i, h_o, k, and r_i remain constant (r_i is roughly the outside radius of the stainless tube ~1.5 mm) while r_o varies, then the rate of heat transfer, q, is a function of r_o alone (which is associated with the thickness of the insulation). The dimensionless form of heat transfer rate is plotted in Fig. 7 as a function of r_o. From Eq 5, the critical radius, $r_{critical}$, for maximum heat transfer can be obtained by setting $dq/dr_o = 0$.

$$r_{critical} = \frac{k}{h_o} \quad \text{(Eq 6)}$$

As we increase the radius (or thickness) of the insulation around the injector, the heat transfer from the hot gas to the injector through the insulation material increases. While seemingly counterintuitive, this is nonetheless a rational result since the increase in the thickness of insulation would also lead to increased surface area in contact with the primary gas flow. As shown in Fig. 7, the amount of heat transfer continues to increase until the radius of the insulation reaches the "critical radius of the insulation," $r_{critical} = k/h_o$. The critical radius of our test case

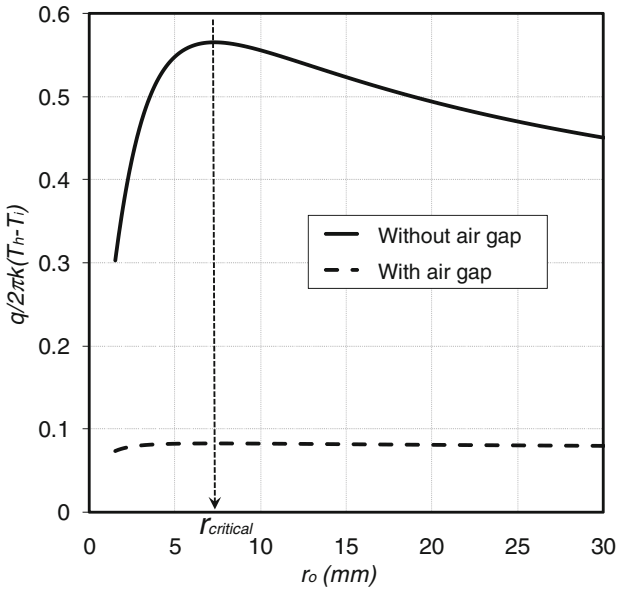

Fig. 7 The normalized heat transfer rates with the thickness of insulator (Macor) with and without air gap

becomes 7.3 mm. Taking $r_i = 1.5$ mm into consideration, this means that the desired Macro thickness should be much larger than 5.8 mm. Since the size of the injector is limited by the size of the prechamber, this is not a practical solution. To avoid this dilemma, a small air gap was introduced between the injector and the Macor with a relatively small thickness to represent a thermal contact resistance, h_c. The contact resistance, h_c, can be approximated with the air gap of 0.1 mm with the thermal conductivity of air, k_a, as shown in Eq 7. The total heat transfer rate in the radial direction per unit length of the tube can be derived as Eq 8. The dimensionless form of the heat transfer rates with an air gap and without an air gap is compared in Fig. 7. As shown in Fig. 7, the heat transfer rate is less sensitive with the thickness of Macor tube. Taken the need for mechanical integrity into consideration, the Macor hollow tubes we used are typically machined to thicknesses of 1 to 2 mm.

$$h_c = \frac{k_a}{r_i \ln\left(\frac{r_i + 0.1}{r_i}\right)} \quad \text{(Eq 7)}$$

$$q = \frac{2\pi(T_h - T_i)}{\frac{1}{h_o r_o} + \frac{1}{h_c r_i} + \frac{1}{k}\ln\left(\frac{r_o}{r_i}\right)} \quad \text{(Eq 8)}$$

Assuming a Macor tube thickness of 1.0 mm, the computed gas velocity vectors and the temperature distribution are shown in Fig. 8. The temperature distribution does not appear to be strongly affected by the thickness of Macor tube due to the thermal contact resistance of the air gap explained in Fig. 7. This can be illustrated from the simulation results shown in Fig. 9, which compares three different Macor wall thicknesses: $t = 0$ (i.e., no insulation), $t = 0.5$, and $t = 1.7$ mm. Clearly,

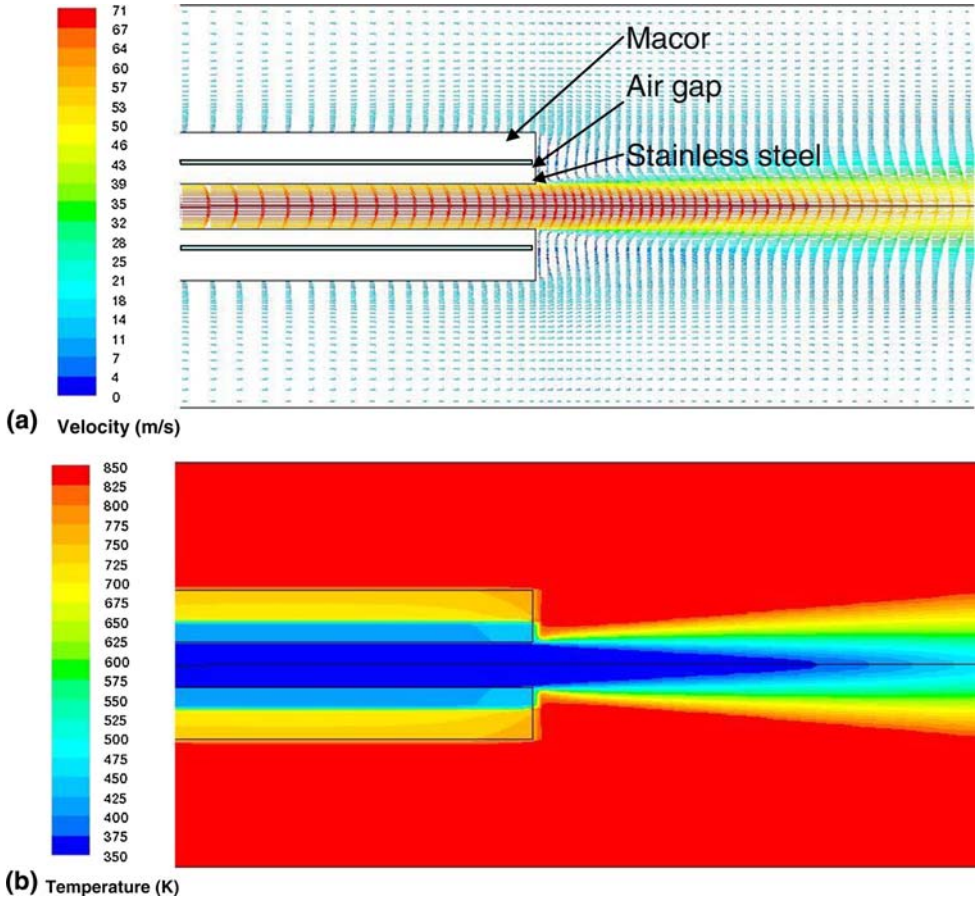

Fig. 8 Simulated distributions of gas flow (a) and temperature (b) for the injector configuration shown in Fig. 4(b), assuming that the air gap is assumed 0.1 mm and Macor wall thickness is 1.1 mm

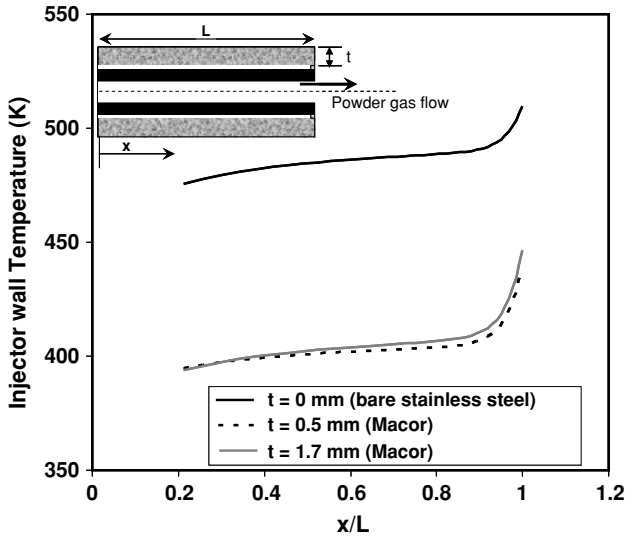

Fig. 9 Effects of Macor insulation thickness for the injector configuration shown in Fig. 4(b). The air gap is assumed to be 0.1 mm

the effect of the thicknesses of the insulation is relatively small. The injectors with thicknesses of 0.5 and 1.7 mm of Macor produced roughly 80 K lower wall temperatures than the bare stainless steel injector throughout most of the injector length. It can be also noted from the simulation result in Fig. 9 that the injector wall temperature increases sharply near the exit end of the injector. This explains the fact that the powder buildup/injector clogging invariably initiates near the exit of the injector (e.g., see Fig. 5). To further mitigate the effect of this higher temperature segment, two recessed injector configurations are examined in the following section.

4.3 Improved Injector Configurations

As shown in Fig. 4(c), the recessed configuration was assembled with cement similar to the basic configuration shown in Fig. 4(b). The inside diameter of the Macor tube was machined about 200 μm larger than the outside diameter of the stainless steel tube, thus allowing a loose fitting between them. Two recessed configurations (1.7 and 3.8 mm recess lengths) were also simulated using Fluent CFD analysis, which indicated a significant temperature decrease near the exit of the injector, compared to the basic configuration in Fig. 4(b). Figure 10 shows the gas velocity and the temperature distributions for the recessed configuration with 3.8 mm recess length. It indicates that the configuration with the recess is very effective to lower the temperature near the exit end of the

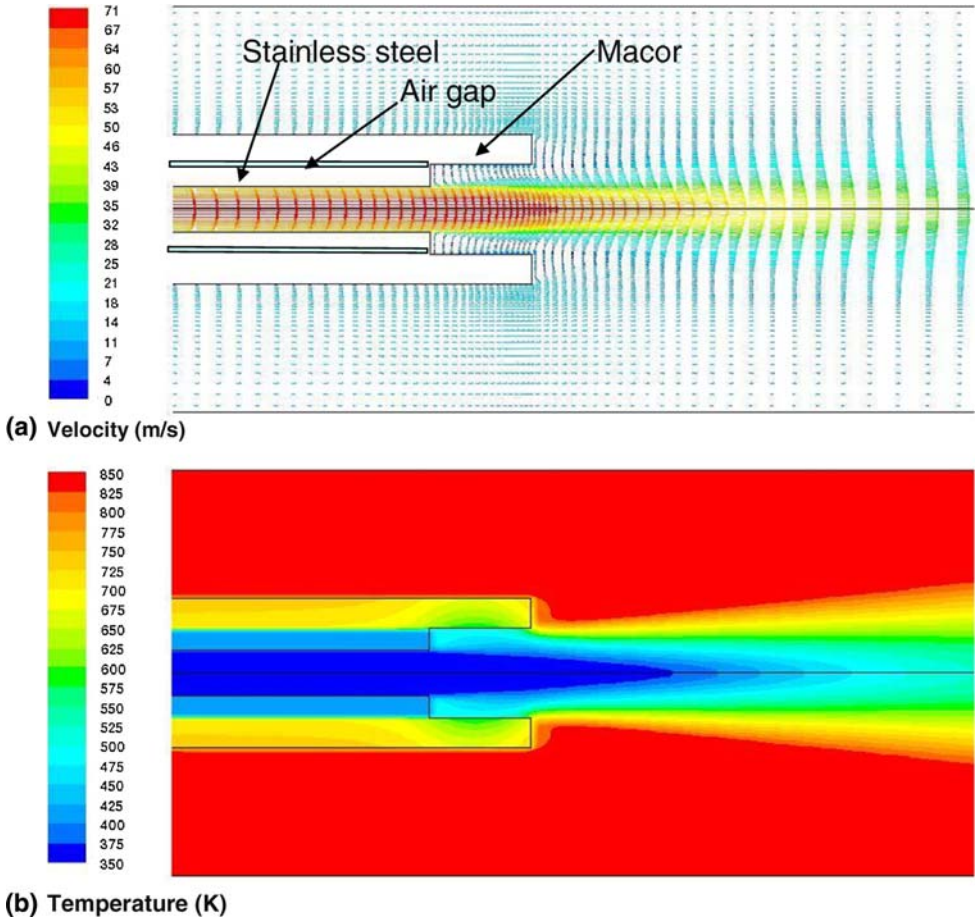

Fig. 10 Simulated distribution of gas flow (a) and temperature (b) for the injector configuration shown in Fig. 4(c). The recess length is assumed to be 3.8 mm

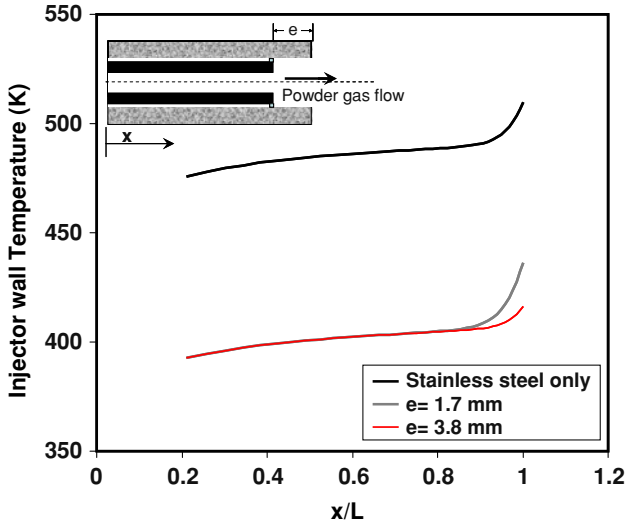

Fig. 11 Simulation results for the effects of recess length on the injector wall temperature

injector. The simulation results for two different recess lengths were also compared with the baseline case for the bare stainless injector. As shown in Fig. 11, the longer recess configuration seems to be effective in lowering the temperature at the exit end of the injector. In comparison with the case with bare stainless steel tube, the wall temperature of the injector dropped by nearly 100 K by introducing the recessed configuration with 3.8 mm recess length. The injector made with such configuration was tested in spraying Al alloys at primary gas temperatures up to 920 K. There was no indication of a decrease in powder gas flow (a primary signature for injector buildup/clogging) after spraying the material for hours. It can be observed from the SEM micrograph in Fig. 12 that little powder particles buildup on the interior surfaces of the injector after several hours of spray time. As discussed in section 4.4, the improved injector allows one to use spraying conditions that are favorable to coating formation while still maintaining steady, clogging-free powder injection.

4.4 Effects of Powder Injection on Coating Formation

With the improved injectors, it becomes possible to use spraying conditions that are favorable to coating formation, while still maintaining steady, clogging free powder injections. The powder gas flow is controlled primarily by

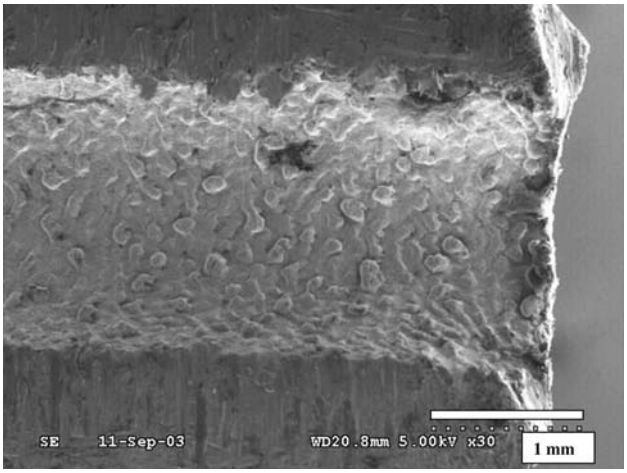

Fig. 12 SEM micrograph showing the interior wall surface of an injector after use for months at main gas temperature of 870 K. The image is taken from the section near the exit, where the highest temperature occurs during operation

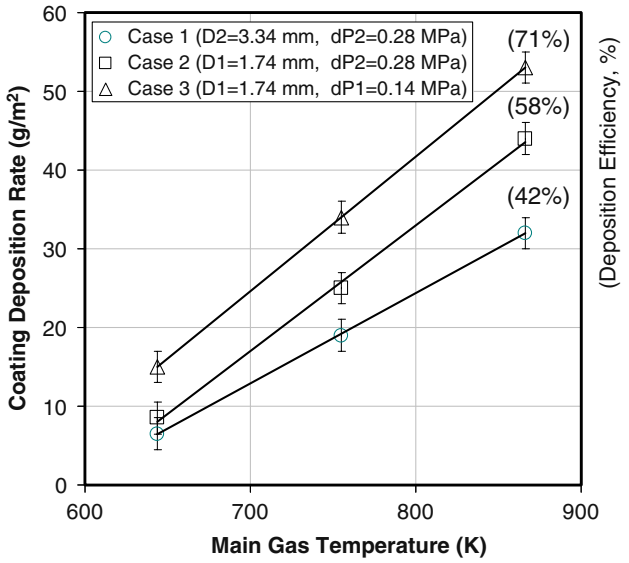

Fig. 13 The coating deposition rate of Al alloy coatings, showing the effects of powder injector and pressure differential ($\Delta P = P_2 - P_1$) on coating formation. During coating deposition, the substrate was traversed at the speed of 0.8 m/s. The conditions for the three cases are listed in Table 2

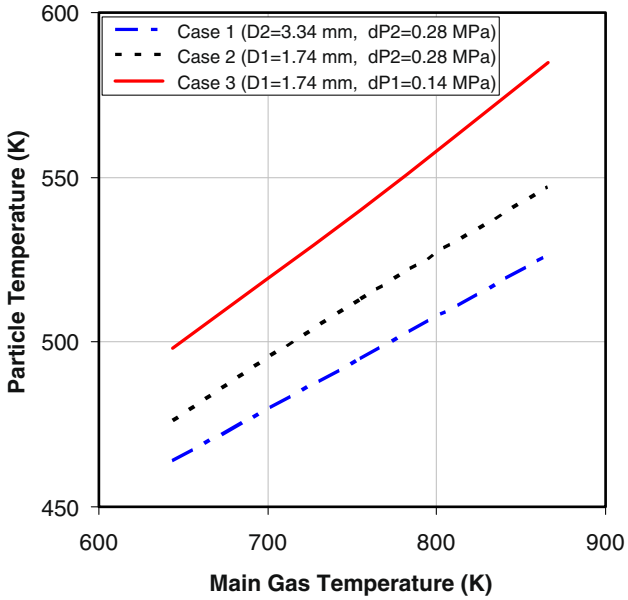

Fig. 14 Simulated particle temperatures at the downstream of the mixing chamber (at the entrance of the converging/diverging nozzle). Fifty-five μm size Al-Si particles were used for simulation. The conditions for the three cases are listed in Table 2

the size of the injector and the differential pressure between the powder feeder and the prenozzle chamber. Since the injector is largely submerged inside the heated gas flow, a sufficient powder gas flow is needed to prevent the injector from buildup/clogging by particles. However, too much powder gas flow can degrade coating formation. The carrier gas is actually a mixture of the heated main gas and the room temperature powder feed gas. Only the main gas is heated to elevated temperatures and the powder feed gas is at a room temperature. To illustrate the effects of the different powder injectors and the related injection conditions on coating formation, the spraying results of Al-Si alloys with two different injectors under different injection conditions were compared. The powder injection-related spraying parameters were summarized in Table 2. With the configuration as shown in Fig. 4(c), a steady powder injection could be achieved with powder gas flow of 4.7 g/s (~8 cfm) at $\Delta P = 0.14$ MPa (~20 psi) without particle buildup and injector clogging. The effects of the different powder injectors and the related injection conditions on coating formation were shown in Fig. 13. All coatings were deposited onto 18 × 740 mm^2 Al substrates. The coating deposition rate represents the amount of coating per unit area and it is directly proportional to the deposition efficiency of the coating. The deposition efficiencies of the coatings deposited at 860 K are also given in Fig. 13. It can be seen that the Case 3 with a small injector and, particularly, with a lower differential pressure, leads to significantly increased deposition efficiency.

To explain the effects of powder gas flow on the coating formation, it was simulated for the three cases of studies listed in Table 2. The particle temperatures are affected by both the effective temperature of the gas stream (i.e., the mixture of the primary gas and the powder feed gas) and the residence time of particle within the gas stream before entering into the spray nozzle. The calculated particle temperatures for the three cases are shown in Fig. 14. The simulated results appear to correlate very well with the experimental data in Fig. 13. Note that the Case 3, with a smaller injector along with a lower differential pressure, resulted in significantly increased particle temperature. Relatively, low particle velocities at the prenozzle chamber were very effective to raise the particle temperatures due to high particle residence time. Furthermore, the decreased powder gas flow in this case also gave rise to higher effective carrier gas temperatures at

the nozzle inlet. The higher effective gas temperature at the entrance of the converging/diverging nozzle resulted in increased particle velocities at the nozzle exit which were simulated and discussed in the previous work (Ref 8). For the smaller injector with lower differential pressures conditions, the cause for the enhanced coating formation was primarily due to increased particle temperatures and supplemented with increased particle velocities at the nozzle exit that was associated with the higher effective carrier gas temperature at the entrance of the converging/diverging nozzle.

5. Summary and Conclusions

Powder clogging issues in the powder injector were investigated through both experimental studies and computational simulations. When spraying difficult-to-deposit material using compressed air or nitrogen as propellant gas, the primary gas is commonly heated to elevated temperature up to 1000 K. This is often a necessity to achieve sufficient particle velocity and particle temperature for enhanced coating formation. Under these conditions, the powder injector, which is in direct contact with primary gas, can be subject to powder particle buildup. This causes continuous deviations of spray parameters from the operating set-points and eventually results in complete clogging of the injector. It is recognized that injector clogging is caused primarily by relatively high surface temperatures experienced by the injector interior surface. Examinations of several new injector configurations by both computational simulations and experimental test lead to identification of the improved injector configurations. This study for various injection configurations that resulted in an improved coating formation lead to the following benefits:

a. Enables one to operate the high-pressure cold spray process at increased primary gas temperatures.
b. Allows the use of less powder gas flow without clogging the injector, thus increasing the effective temperature of propellant gas.
c. One can use the powder injection conditions that increase the dwell time of sprayed particles inside the heated gas stream before the converging/diverging nozzle and, therefore, increasing the particle temperatures.

References

1. A.P. Alkhimov, A.N. Papyrin, V.F. Kosarev, N.I. Nesterovich, and M.M. Shushpanov, Gas Dynamics Spraying Method for Applying a Coating, U.S. Patent 5,302,414, 12 April 1994
2. R.C. McCune, A.N. Papyrin, J.N. Hall, W.L. Riggs, and P.H. Zachowski, An Exploration of the Cold Gas-Dynamics Spray Method for Several Materials Systems, *Thermal Spray Science and Technology*, C. C. Berndt and S. Sampath, Ed., ASM International, Materials Park, OH, 1995, p 105
3. R.C. Dykhuizen, M.F. Smith, D.L. Gilmore, R.A. Neiser, X. Jiang, and S. Sampath, Impact of High Velocity Cold Spray Particles, *J. Therm. Spray Technol.*, 1999, **8**, p 559
4. T.H. Van Steenkiste, J.R. Smith, R.E. Teets, J.J. Moleski, and D.W. Gorkiewicz, Kinetic Spray Coating Method and Apparatus, U.S. Patent 6,139,913, 31 Oct 2000
5. T.H. Van Steenkiste, J.R. Smith, R.E. Teets, J.J. Moleski, D.W. Gorkiewicz, R.P. Tison, D.R. Marantz, K.A. Kowalsky, W.L. Riggs, P.H. Zajchowski, B. Pilsner, R.C. McCune, and K.J. Barnett, Kinetic Spray Coatings, *Surf. Coat. Technol.*, 1999, **111**, p 62
6. T.H. Van Steenkiste, J.R. Smith, and R.E. Teets, Aluminum Coatings via Kinetic Spray with Relatively Large Powder Particles, *Surf. Coat. Technol.*, 2002, **154**, p 237
7. T.H. Van Steenkiste and J.R. Smith, Evaluation of Coatings Produced via Kinetic and Cold Spray Processes, *J. Therm. Spray Technol.*, 2004, **13**, p 274
8. T. Han, Z. Zhao, B. Gillispie, and J.R. Smith, Effects of Spray Conditions on Coating Formation by the Kinetic Spray Process, *J. Therm. Spray Technol.*, 2005, **14**, p 373
9. Z.B. Zhao, B.A. Gillispie, and J.R. Smith, Coating Deposition by the Kinetic Spray Process, *Surf. Coat. Technol.*, 2006, **200**, p 4746
10. B.E. Launder and D.B. Spalding, The Numerical Computation of Turbulent Flows, *Comput. Methods Appl. Mech. Eng.*, 1974, **3**, p 269-289
11. *Fluent 6.2, Commercial CFD Code*, Fluent Inc., Lebanon, NH, 2005
12. D.L. Gilmore, R.C. Dykhuizen, R.A. Neiser, T.J. Roemer, and M.F. Smith, Particle Velocity and Deposition Efficiency in the Cold Spray Process, *J. Therm. Spray Technol.*, 1999, **8**, p 576
13. R.C. Dykhuizen and M.F. Smith, Gas Dynamic Principles of Cold Spray, *J. Therm. Spray Technol.*, 1998, **7**, p 205
14. W.M. Rohsenow and H. Choi, *Heat, Mass, and Momentum Transfer*, Prentice Hall, Englewood Cliffs, NJ, 1961